Numerical modeling of RC beams strengthened with CFRP under dynamic loading

S.Mohammadi , A.A.Mousavi Khandan
Civil Department, Faculty of Engineering, University of Tehran, Tehran, Iran

ABSTRACT: In recent years, strengthening of tensile face of reinforced concrete beams with fiber reinforced polymer (FRP) sheets has been increased as a popular approach for flexural strengthening of reinforced concrete (RC) beams. This paper presents a combined finite/discrete element method based on 2D and 3D modeling of a strengthened RC beam subjected to dynamic loadings. Complexity of interaction of different contact elements in the form of discrete element method and taking to account all failure criteria including cracking in concrete or delamination of CFRP composite laminates from concrete substrate and etc. makes it necessary to do such an analysis for considering complex mechanism of failure. The proposed approach adopts a node to face contact based delamination control to simulate the inter-FRP-RC interactions. The validity of developed algorithm is verified by solving available standard and experimental tests from the literature.

1 INTRODUCTION

Different approaches have been developed to retrofit existing structures due to their damage by loads higher than the design service loads, or by chemical processes due to aggressive environmental conditions. Plate bonding for structural strengthening was utilized in the early 1960's and was used primarily in France and South Africa. Klaiber et al. (1987) & Lander et al. (1981) studied the use of epoxy-bonded steel plates to strengthen bridge girders in Europe, South Africa, and Japan. Later, in 1982 the technique of applying fiber reinforced polymer (FRP) sheets to the tensile face of reinforced concrete (RC) beams were developed for flexural strengthening by Meier (1978) in Switzerland. Because of unique advantages of FRP composites in comparison to the conventional steel bars and plates, such as high strength-to-weight ratio and considerably good resistance to corrosion, they have been widely applied to the strengthening and upgrading of structurally inadequate or damaged concrete structures. Later, the effectiveness of glass-FRP plates bonded to the tension face of the RC beams was experimentally investigated by Saadatmanesh & Ehsani (1991). Extensive research has been carried out on the numerical modeling of concrete beams strengthened by FRP composite. Although finite element analyses (FEA) have been carried out on plated RC beams (Zhang et al. 1997, Ziraba 1995, Arduini et al. 1995, Quantrill et al. 1995, He et al. 1997, Jerome et al. 1997, Rahimi et al. 2001), little success has been made in simulating debonding failures, especially for beams which are under dynamic loads. This is primarily because of the complexity of the problem and the interaction of different interfaces between concrete, steel, FRP plate and adhesive layer. The problem becomes extremely difficult when the RC beam is loaded dynamically, where different geometry, stiffness and interaction between the interfaces before and after debonding or cracking of the RC beam is expected in any new time step. Therefore, adopting a proper debonding model for the adhesive layer and a fracture criterion for concrete cracking is essential for an accurate simulation. In FEA, there are two major approaches representing cracking in concrete structures; discrete and smeared crack approaches. The smeared crack approach which defines a reduced equivalent continuum has some deficiencies such as mesh sensitivity, incapability for taking into account the new geometry and its trend to spread the crack formation over a region of the structure so unable to accurately predict the local fracture failures (Rahimi & Hutchinson 2001). The other essential part of the simulation is the bonding/ debonding behavior of the adhesive layer. In recent years, many efforts have been made to study the interfacial bonding/debonding behaviors. Taljsten theoretically derived a linear equation that calculates the load carrying capacity of FRP-bonded concrete prism under uniaxial tensile loading. More

investigations of FRP-concrete interfacial bond models were reported by Yuan et al. (2001) and Nishida et al. (1999), in which several types of nonlinear shear stress versus relative displacement (τ-δ_l) relationships were proposed.

By examining the results of a wide range of experimental tests, debonding failures in flexurally strengthened RC beams may be broadly classified into two types: plate end debonding (including cover separation failure and plate end interfacial debonding) in which failure starts from one of the plate ends due to local stress concentration, and intermediate crack induced debonding in which debonding starts from either a flexural crack or a flexural shear crack (Teng et al. 2002). In the cover separation failure microdiagonal cracks that occur in the interfacial concrete finally connect together and lead to the delamination of FRP sheets (Fig. 1b). In this case, it is assumed that the bond strength of adhesive layer is relatively high. The other type of debonding happens within epoxy adhesive layer, which is mainly due to weak or imperfect bond (Fig 1a). In both of these cases one flexural crack locally occurs at mid span from which the debonding initiates and propagates, no matter if the interfacial debonding happens within adhesive layer or though interfacial concrete. The second major type of debonding is schematically shown in Figure 1c, in which a secondary diagonal shear or flexural crack occurs beside the first flexural concrete crack at mid span. Then, the debonding starts to propagate from the root of the secondary diagonally shear or flexural crack (Zhishen et al. 2003).

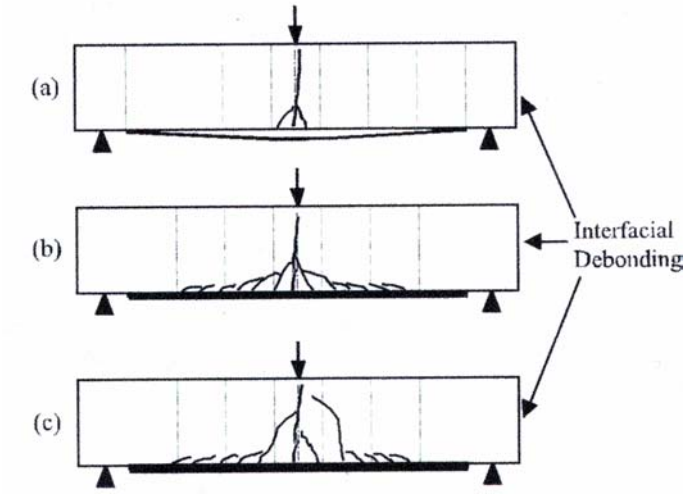

Figure1. Interfacial debonding failure mode (Zhishen et al. 2003)

In this study, a new approach has been developed which utilizes a combined finite/discrete element method. The proposed algorithm consists of full material and geometry non-linearities. The Sprenger (Sprenger et al. 2000) criterion is adopted for modeling the bonding behavior of FRP-concrete interface. To verify the performance of the proposed algorithm an experimentally tested RC beam subjected to dynamic loading is simulated and the results will be discussed (Jerome et al. 1997).

2 PRINCIPLES OF MODELING

In this simulation, a combined finite/ discrete element method is utilized. All types of non-linearity in material or geometry are considered in this study. Using an "explicit central difference time integration technique" reduces the time of computation, especially for large models. Cracking in the concrete material is considered using a non-linear fracture mechanic method on the basis of plasticity theory and utilizing discrete elements.

The discrete element method, utilizes the principles of penalty based contact mechanics enforcing virtual springs to tie degrees of freedom. Also for modeling bonding/debonding behavior of FRP-concrete interface a mixed mode model was used on the base of Hashin criterion with a bilinear strain softening model.

The use of discrete elements in problems with changing geometry in successive time steps, with its capability of remeshing and adaptivity, provides us with a powerful numerical tool for modeling complex problems. In fact, creation and propagation of crack in a structure can be geometrically followed by remeshing of the finite elements (Mohammadi 2003).

For 3D problems, mixed mode debonding model of FRP-concrete interface developed and Drucker-Prager material model was used in concrete. The overall failure of the model was investigated by monitoring the maximum principal stress.

3 MATERIAL MODELING

There are three major fracture and failure behavior in concrete structures strengthened with FRP composites. So, it's essential to assume proper material models and a suitable delamination criterion in order to conduct a successful simulation.

3.1 *Concrete material model*

The compressive behavior of concrete was modeled by Drucker-Prager material model and an associated flow rule. The Rankine fracture model is utilized to model the concrete behavior in tension while a bilinear strain softening relation is adopted for a smooth non-local release of energy.

3.2 *CFRP material model*

The behavior of CFRP is assumed to be linear elastic and orthotropic till unidirectional CFRP sheets reach

their tensile strength as no rupture in CFRP sheets has been reported in experimental tests (Jerome et al. 1997).

3.3 *Material model for FRP-concrete interface*

Debonding in FRP-concrete interface is one of the major failure modes in strengthened RC beams. In the proposed algorithm, a 3D Hashin model is adopted to predict initiation of interfacial debonding. Primary model has established on the base of softening time independent plasticity model.

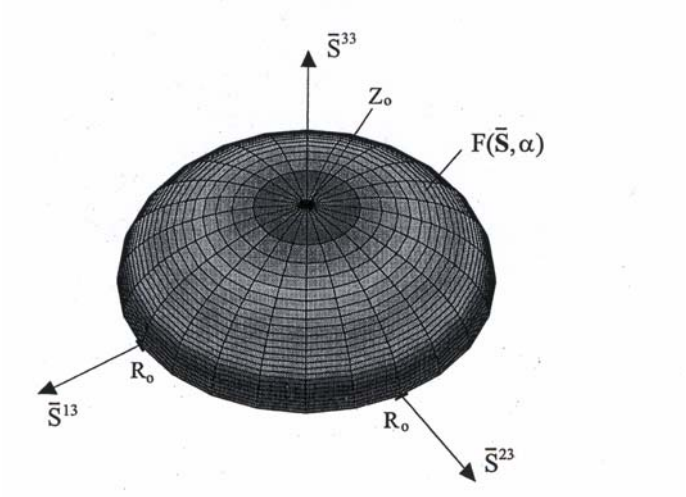

Figure2. Delamination criterion of Hashin

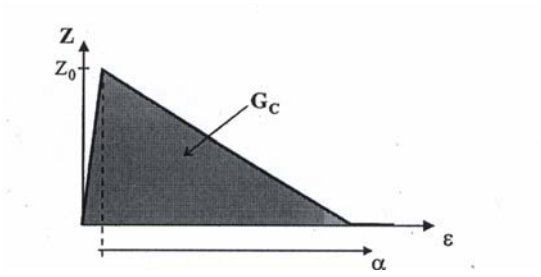

Figure3. Softening function

Assuming large deformations (though small strains), the rate of the Green-Lagrangian strain tensor is decomposed into an elastic and an inelastic parts. The inelastic strain rate follows the associated flow rule:

$$\dot{\bar{E}} = \dot{\bar{E}}^{el} + \dot{\bar{E}}^{in} \tag{1}$$

$$\dot{\bar{E}}^{el} = \bar{C}\dot{\bar{S}} \tag{2}$$

$$\dot{\bar{E}}^{in} = \dot{\bar{E}}^{pl} = \dot{\lambda}\frac{\delta F}{\delta \bar{S}} \tag{3}$$

Here, $\bar{C}$ is the elasticity matrix for plane isotropic behavior of the material. $\bar{S}$ is the stress matrix, λ is the inelastic coefficient and F is the yield function.

The Hashin delamination criterion is a function of interlaminar stresses $\bar{S}^{33}, \bar{S}^{13}, \bar{S}^{23}$, tensile strength in direction of the thickness Z_0 and tangential strength of layer R_0.

$$\frac{\left(\bar{S}^{33}\right)^2}{{Z_o}^2} + \frac{\left(\bar{S}^{13}\right)^2 + \left(\bar{S}^{23}\right)^2}{{R_o}^2} \le 1 \tag{4}$$

A plot of the criterion is shown in Figure 2. The yield function $F(\bar{S},\alpha)$ is obtained by reformulation of the delamination criterion:

$$F\left(\bar{S},\alpha\right) = g\left(\bar{S}\right) - Z\left(\alpha\right) \le 0 \tag{5}$$

$$g\left(\bar{S}\right) = \sqrt{\bar{S}^T A \bar{S}} \tag{6}$$

$$A = \begin{bmatrix} 0 & 0 & 0 & 0 & 0 & 0 \\ 0 & 0 & 0 & 0 & 0 & 0 \\ 0 & 0 & 1 & 0 & 0 & 0 \\ 0 & 0 & 0 & 0 & 0 & 0 \\ 0 & 0 & 0 & 0 & \left(\frac{Z_o}{R_o}\right)^2 & 0 \\ 0 & 0 & 0 & 0 & 0 & \left(\frac{Z_o}{R_o}\right)^2 \end{bmatrix} \tag{7}$$

$Z(\alpha)$ is a linear softening function as follows:

$$Z\left(\alpha\right) = Z_o\left(1 - \mu\alpha\right) \tag{8}$$

And it is depicted in Figure 3. The variable α can be assumed as the equal inelastic strain. The parameter μ describes the slope of the softening function $Z(\alpha)$. It is a material parameter and can be determined from the critical energy release rate G_c, tensile strength Z_0 and the thickness of the intermediate layer h_T:

$$\mu = \frac{Z_o \times h_T}{2G_c} \tag{9}$$

The rate of the internal variable is defined with the evolution law:

$$\dot{\alpha} = -\dot{\lambda}\frac{\partial F}{\partial Z} \tag{10}$$

The gradient of the yield function is derived as follows:

$$\frac{\partial F}{\partial \bar{S}} = \frac{1}{g\left(\bar{s}\right)} A\bar{S} = N, \frac{\partial F}{\partial Z} = -1 \tag{11}$$

Substitution of Equation 11 into Equations 1-3 and introducing a backward Euler integration algorithm within a time step $t_{n+1} = t_n + \Delta t$ yields:

$$\bar{E}_{n+1} = \bar{C}^{-1}\bar{S}_{n+1} + \bar{E}_n^{\,pl} + \frac{\lambda}{g\left(\bar{S}_{n+1}\right)} A\bar{S}_{n+1} \tag{12}$$

$$\bar{S}_{n+1} = \left[\bar{C}^{-1} + \frac{\lambda}{Z\left(\alpha_{n+1}\right)} A\right]\left[\bar{E}_{n+1} - \bar{E}_n^{\,pl}\right] \tag{13}$$

$$\bar{S}_{n+1} = P\bar{E}^{tr} \tag{14}$$

Where subscripts n and n+1 denote the quantities of the known converged configuration at time t_n and t_{n+1}, respectively. Updating the internal parameter α is performed using a backward Euler integration:

$$\alpha_{n+1} = \alpha_n + \lambda \tag{15}$$

Linearization of the stress tensor has to be derived for the finite element formulation. After some algebric manipulations we end up with the consistent tangent matrix:

$$\overline{D} = P - \frac{PN(PN)^T}{N^T PN + H} \tag{16}$$

With:

$$H = \frac{Z'}{1 - \lambda \dfrac{Z'}{Z}} \text{ , and } Z' = -\mu \tag{17}$$

4 NUMERICAL SIMULATION

Different classes of problems are simulated to assess the performance of the proposed algorithm. The first one examines the debonding phenomenon in a buckling analysis of a composite panel, and the second one simulates an experimental CFRP strengthened RC beam.

4.1 Numerical simulation of a composite beam

A pre-cracked unidirectional composite panel as depicted in Figure 4 is subjected to an incrementally increasing loading until the local and global buckling modes occur (Mohammadi & Forouzan-sepehr).

Figures 5 and 6 show the predicted buckling modes, where the local and global buckling modes occurred at loads 1410 lbf/in (246.93 N/mm) and 7310 lbf/in (1280.18 N/mm), respectively. The results are comparable to the loads 1312 lbf/in (229.77 N/mm) and 7821 lbf/in (1369.67 N/mm), reported by Progini (Fig. 6).

4.2 Example beam and material properties

A strengthened RC beam, reportedly tested by Jerome & Ross (1997), was analyzed in this study. The dimensions of the simply supported beam were

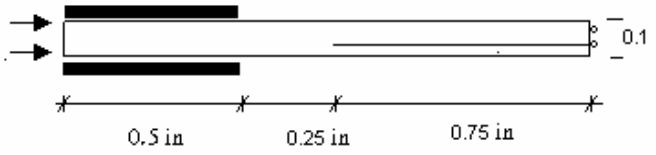

Figure 4. Geometry of a composite panel with an initial interlaminar crack

Table 1. Material Properties of Composite Panel

Parameter	Value		Parameter	Value	
	ksi	MPa		lbf/in.	N/mm
E_{xx}	20200	139274.1	G_{IC}**	0.5	0.0876
E_{zz}	1410	9721.6	G_{IIC}**	0.5	0.0876
E_{yy}	1410	9721.6			
G_{xy}	810	5584.75		Unitless	
G_{yz}	546	3764.54	ν_{yz}	0.29	
X_T*	220	1516.85	ν_{xy}	0.29	
Y_T*	6.46	44.54	ν_{xz}	0.29	
X_C*	231	1592.69			
Y_C*	36.7	253.04			
S*	15.5	106.87			

* Parameters of Hoffman yield criterion

** Fracture energy release rate

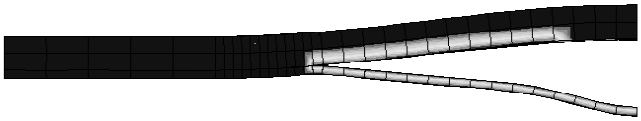

Figure 5. Local and global buckling modes

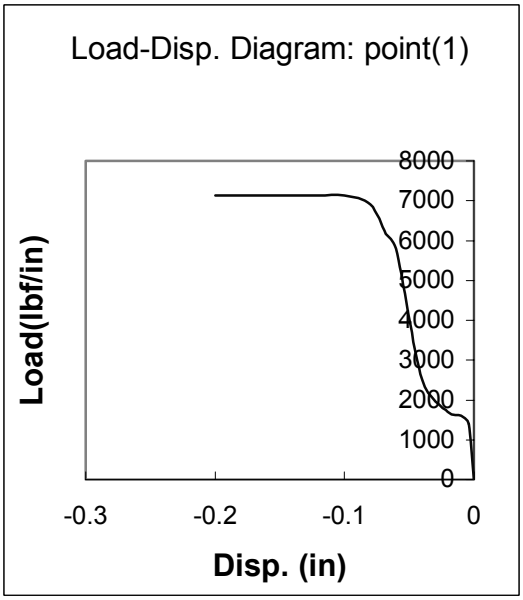

Figure 6. Displacement versus time in local and global buckling modes

3×3×30 in (7.62×7.62×76.2 cm). There was no tensile steel in the beam, while the beam was strengthened by CFRP panels.

The size of the CFRP panels was 3×30 inch and each was composed of three plies. The adhesive material used to bond CFRP panels was a thixotropic, modified, two part epoxy.

In order to determine the dynamic behavior of beams externally reinforced with CFRP panels, a series of drop-weight center-point loading were conducted (Jerome et al. 1997). Dynamic loading curve versus time was achieved by converting voltage-vs-time signal of a series of electrical resistance strain-gages to load-vs-time signal as shown in Figure 7.

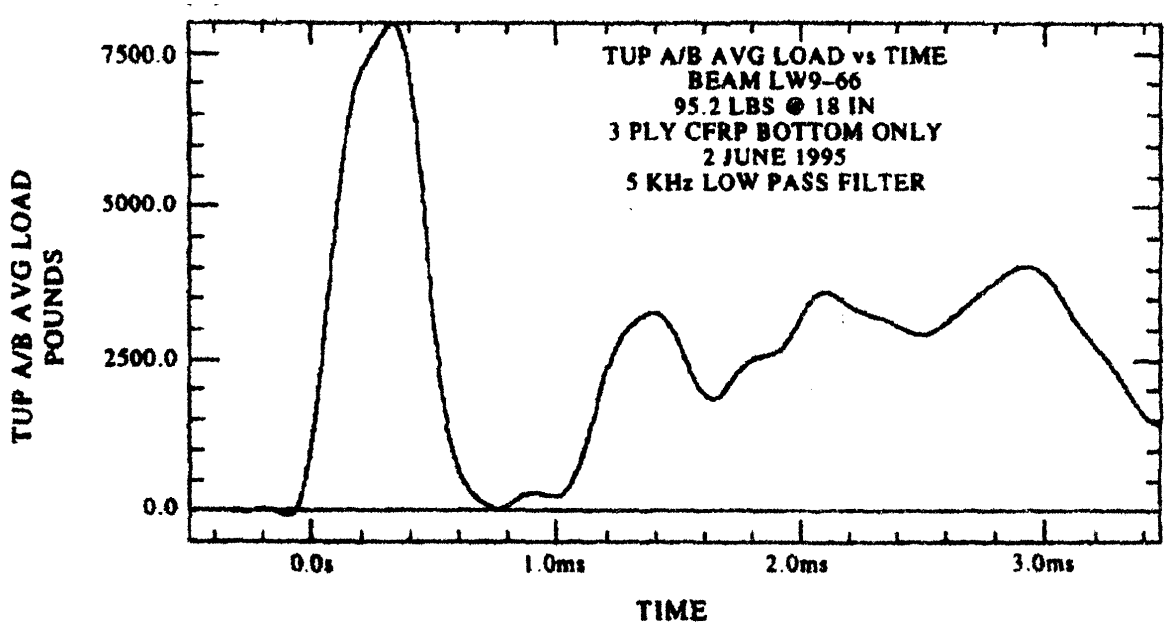

Figure 7. Tup load-time curve (Jerome et al. 1997)

Table 2. Concrete material model parameters

Parameter	Value
E_0 (initial tangent modulus)	2.4×10^4 MPa
υ(Poisson's ratio)	0.2 (unitless)
f_t (Uniaxial cut-off tensile strength)	4.35 MPa
f_c (Uniaxial maximum compressive strength)	46.4 MPa
σ_t (Uniaxial ultimate compressive strength)	39.5 MPa
ρ (mass density)	1892.7 kg/m^3

Table 3. CFRP material model parameters

Parameter	Value
0° Tensile strength	2206.9 MPa
0° Tensile strength	137.9 GPa
Fiber volume	60 %
Cured three-ply thickness	0.4953 mm
ρ (mass density)	1577.25 kg/m^3

Properties of concrete and CFRP panels used in this test are given in Tables 2 & 3. Experimental observations showed that final failure in strengthened concrete beams using CFRP tensile sheets was flexural cracking of concrete beams at nearly mid span and delamination of CFRP sheets afterwards. The following sections discuss 2D and 3D finite element simulations of the mentioned test.

4.3 Numerical simulation and discussion for 3D

Because of the symmetry of loading and geometry only half of the beam was modeled by assuming suitable boundary conditions as depicted in Figure 8. 8-noded cubic elements were used for modeling of the FRP sheet and concrete beam. In the concrete beam the size of elements were gradually increased due to their distance from bottom of the beam by an increasing ratio of 0.7^{-1} as shown in Figures 8 & 9. No contact interface elements are used in adhesive layer and the contact of adjacent elements was conducted by a node to face contact method. For the concrete part 1200 elements were used and CFRP sheets were composed of 630 8-noded cubic elements.

There is a lack of information for adhesive material. Descriptive Properties of adhesive layer, like fracture energy release rate and bond strength are taken 0.5 N/mm and 4 Mpa respectively.

Delamination of CFRP sheet from concrete beam was approximately started at 470 μs at middle of the beam and propagated toward the support. At 750 μs one fifth of the total length of FRP sheet has been debonded from bottom of the beam as shown in Figures 10 and 11.

As it is observed from Figure 12 the maximum principle stress has exceeded from the tensile strength of concrete in the middle part of the beam which is an indication of occurrence of flexural cracking. The extent of delamination in interlaminar layer to one-fifth length of FRP sheets beside the excess of principle stress from the tensile strength of concrete occurs at 750 μs which is closely similar to the experimental observations by Jerome et al. 1997 where failure of the beam was reportedly occurred at 730 μs.

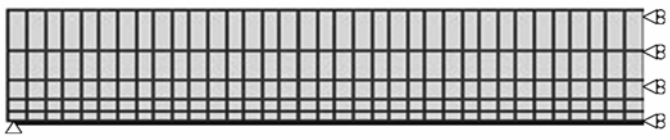

Figure 8. Finite element mesh and boundary conditions

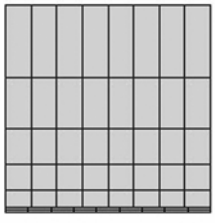

Figure 9. Cross section of the beam

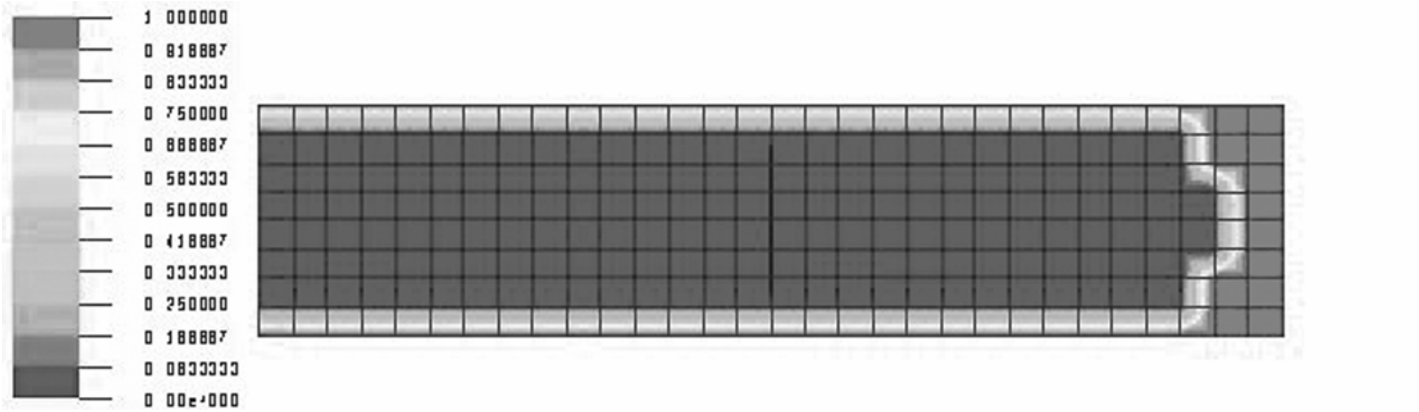

Figure 10. Delamination growth in CFRP plate at time step=.00047 s (0= fully bonded, 1=delaminated)

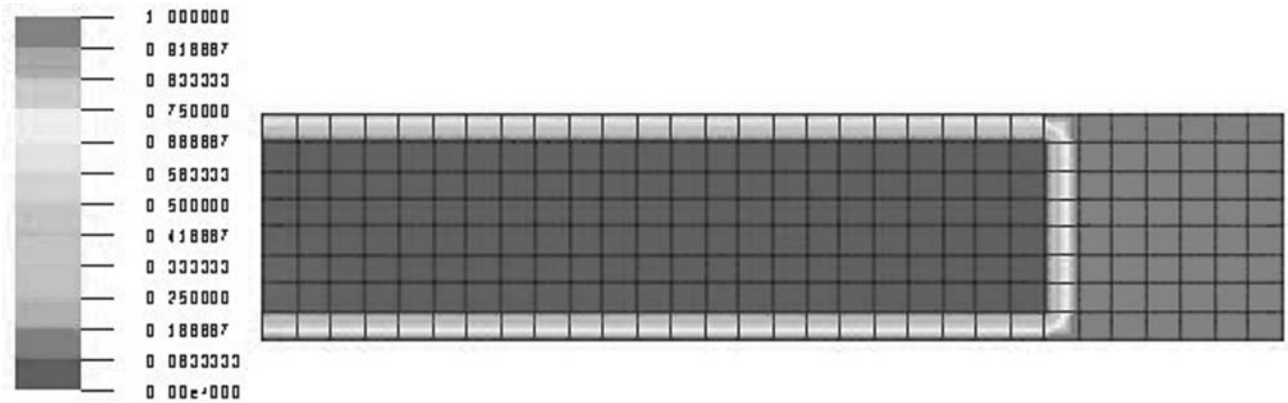

Figure 11. Delamination growth in CFRP plate at time step=.00075 s (0=fully bonded, 1=delaminated)

Figure 12. Contour of maximum principle stress in Pa at time step=.00075 s

The displacement history at mid span of the beam, computed in the numerical analysis, was plotted against the time in Figure 16, marked by circular point compared to full line which shows the displacement resulted from the experimental tests.

The existing differences of resulted displacements in numerical simulation comparing to experimental results, can be attributed to the fact that the simulated beam has more stiffness than the tested beam which is a consequence of elastic behavior of concrete in tensile regime without any tensile fracture. Figures 10 and 11 show debonded region of CFRP sheet from mid span at 470 μs and 750 μs in which bright gray shows the debonded region. Also, Figure 12 shows the maximum principle stress contour at 750 μs.

4.4 Numerical simulation and discussion for 2D modeling

The same beam modeled in section 4.3 is considered. Properties of concrete, CFRP panels and adhesive layer were exactly the same as previous model. As cited in Jerome et al. (1997) it was observed that flexural cracks occurred between 400 μs till 500 μs and by 600 μs, the cracks ran to the upper surface of the beam, which is in a close agreement with results of the performed simulation.

Data, from an strain gage, located on the bottom center of the beam, indicated an abrupt change of slope in the strain-vs-time curve at about 430 μs, indicating crack initiation has occurred. Another strain gage, located on the original neutral axis of the beam also indicated failure at about 430 μs. Another strain gage, located at 2.75 inch (6.985 cm) from the bottom of the beam, showed a change of slope in strain vs. time at about 555 μs, indicating the crack(s) had reached the upper surface of the beam. A post-test damage assessment indicated a single flexural crack had formed at the beam's midpoint.

Analysis was conducted in a plane stress state. Triangular plane stress elements were used for concrete beam and CFRP sheet. The size of these elements varied due to their distance to CFRP sheet, so those elements adjacent to CFRP sheet had a size of 0.001 m and elements adjacent to top of the beam had a size of 0.01 m. The elements of CFRP sheet had a size of 0.00025 m which was decomposed of two layers of elements through the thickness. Details of the mesh are shown in Figure 13. The behavior of CFRP sheet was assumed to be elastic, due to its high strength and the experimental observations. Also, cracking behavior of the concrete beam in tensile regime was taken into account by assuming a Rankine bilinear strain softening model.

The results show that flexural cracks were propagated at the bottom part of mid span at 460μs (Fig. 14). These flexural cracks started to propagate from two distinct origins; both of them were very close to mid span. Later, these cracks started to develop to upper surface of the beam in time interval of 460 μs to 750 μs. They reached to top of the beam at 750 μs (Fig. 15).

Then, at 0.00113 s those distinct cracks were attached to each other. Later, at 0.00127s some signs of delamination were observed at bottom of the beam and at 0.00132 s delamination started to develop gradually.

At 0.00136, flexural cracks attached to each other at middle of the beam, while at 0.00145s, more cracks were appeared and increased. At 0.00165s microcracks started to develop from about mid height of the beam toward the left side (Fig. 17). Propagation of these cracks increased, so that at 0.00171 s they reached to bottom of the beam and it finally created a complete flexural cracking beside microcracks at bottom of the beam (Fig. 18). It is notable that the location where cracks stopped is exactly the same location where delamination of CFRP sheets stopped. It can be seen from the results that the creation and propagation of cracks have occurred at the peak point of the loading.

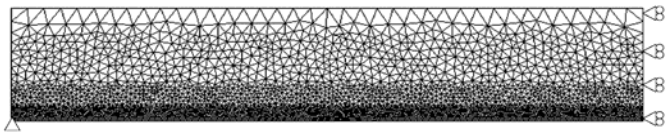

Figure 13. Finite element mesh and boundary conditions

Figure 14. Cracking Pattern at time step=.00046s

Figure 15. Cracking Pattern at time step=.00075s

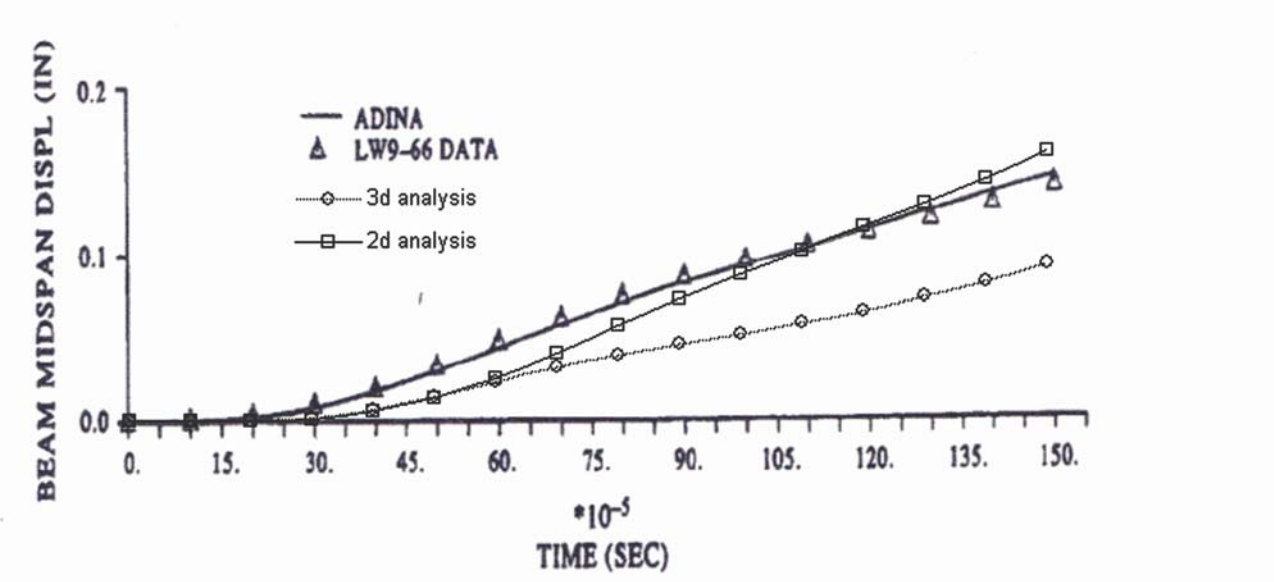

Figure 16. Comparision of mid point displacement vs. time for different solutions

Figure 17. Cracking Pattern at time step=.000165s

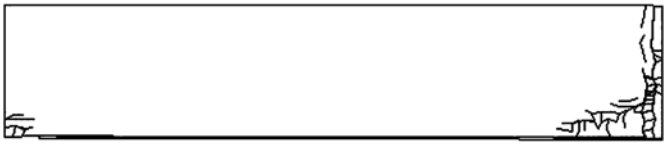

Figure 18. Cracking pattern at time step=.00174s

Also, the displacements computed from the simulations were plotted against experimental displacements at mid span in different time steps with rectangular points marking the displacements computed from the present analysis (Fig. 16). Acceptable agreement between the presemt modeling and tested results is an indicator of the validity of the algorithm.

5 CONCLUSION

This paper has presented a discrete crack model based on finite element analysis method for fiber reinforced polymer (FRP) plated reinforced concrete (RC) beams. A mixed coupling model for simulation of delamination of FRP sheet from concrete substrate was developed on the base of Hashin criterion. The proposed approach adopts a node to face contact based delamination control to simulate the linear-FRP-RC interactions. Conducting analyses in 2D and 3D and comparing the results with the test results showed that flexural cracking continued by delamination of FRP sheet from mid span is a major failure mode of the beam under dynamic loading induced by an impact hammer. In 3D analysis considerable difference in displacements show that assuming a suitable fracture model for concrete is indispensable for true prediction of overall behavior and failure mode. Close agreement between test results and performed analysis showed that the proposed algorithm for modeling this type of problems may effectively be used.

6 REFERENCES

Arduini M, Tommas AD, Manfroni O. 1995. Fracture mechanism of concrete beams bonded with composite plates. In Taerwe L (ed.), *Non-metalic (FRP) reinforcement for concrete structures*: 484-91. E&FN Spon: RILEM

He JH, Pilakoutas K, Waldron P. 1997. Analysis of externally strengthening RC beams with steel and CFRP plates. *Proc. 7th int conf. On structural faults and repairs; Edinburgh*: 83-92.

Jerome DM & Ross CA. 1997. Simulation of the dynamic response of concrete beams externally reinforced with carbon-fiber reinforced plastic. *Comput struct* 64(5/6): 1129-53.

Klaiber, F.W., Dunker,K.F., Wip, T.J., and Sanders, W.W.,Jr., Methods of strengthening existing highway bridges, *NCHRP research report No. 293,Transportation research board, Sep. 1987:11*

Ladner, M. & Weder, C.. Geklebt Bewhrung im Stahlebetonbau, *Report No. 206,1981*. EMPA Dubendorf

Meier, U.. Bridge repair with high performance composite materials. *Material Tech, 1978*, Vol. 4: 125-128.

Mohammadi S. 2003. *Discontinuum mechanics by finite and discrete elements*. UK: WIT.

Mohammadi S. & Forouzan-sepehr S. 2003. 3D adaptive multi fracture analysis of composites. Materials Science Forum 440-441:145-152.

Nishida H, Kamiharako A, Shimomura T, Maruyama K. 1999. Bond mechanism between continuous fiber and concrete. *Proc JCI* 21(3): 1507-12.

Quantrill RJ, Hollaway LC, Throne AM, Parke GAR. 1995. Preliminary research on the strengthening of reinforced concrete beams using GFRP. In Taerwe L (ed.), *Non-metalic (FRP) reinforcement for concrete structures*: 543-50. E&FN Spon: RILEM.

Progini P., Riccio A., Scaramuzzino F. 1999. Influence of Delamination Growth and Contact Phenomena on the Compressive Behavior of Composite Panels. Journal of Composite Materials 33(15): 1433-1465.

Rahimi R & Hutchinson A. 2001. Concrete beams strengthening with externally bonded FRP plates. *ASCE J Compos Constr* 5(1):44-56.

Saadatmanesh, H. & Ehsani, MR. 1991. RC beams strengthened with GFRP plates. I: experimental study. *J Struct Eng* 117(11): 3417-3433

Sprenger W., Gruttmann F., Wagner W. 2000. Delamination growth analysis in laminated structures with continuum-based 3D-shell elements and a viscoplastic softening model. *Comput. Methods Appl. Mech. Engrg* 185: 123-139.

Taljsten B. 1996. Strengthening of concrete prisms using the plate-debonding technique. *Int J Fract 81:253-66.*

Teng JG, Chen JF, Smith ST, Lam L. 2002. *FRP strengthened RC structures*. Chichester: John Wiley and Sons.

Zhang S, Raoof M, Wood LA. 1997. Prediction of peeling failure of reinforced concrete beams with externally bonded plates. *Proceedings of the Institution of Civil Engineers. Struct Build* 122:493-6.

Zhishen Wu & Jun Yin. 2003. Fracturing behaviors of FRP-strengthened concrete structures. *Eng Fract Mech* 70: 1339-1355.

Ziraba YN. 1995. Computational model for reinforced concrete beams strengthened by epoxy bonded steel plates. *Finite Elem Anal Des* 12(4): 203-19.

Yuan H, Wu ZS, Yoshizawa H. 2001. Theoretical solution on interfacial stress transfer of externally bonded steel/composite laminates. *J Struct Mech Earthquake Eng JSCE* 4:27-39.